

Sensor placement optimization for guided wave-based structural health monitoring

Hossein Hosseini-Toudeshky^a and Fazel Abdolrezaei Amjad*

Department of Aerospace Engineering, Amirkabir University of Technology, 424, Hafez Ave, Tehran, Iran

(Received June 4, 2019, Revised August 7, 2020, Accepted April 27, 2021)

Abstract. Sensor placement optimization is an attempt to reduce the cost and enhance the detection performance in structural health monitoring (SHM) systems. This paper aims at studying sensor placement optimization for SHM systems. The attention is paid to lamb wave or guided wave-based SHM (GWSHM). By using detection theory and Bayes risk framework the expected cost (loss) of decision making or Bayes risk for SHM system is minimized and the optimal detector is derived. The global detection and false alarm rate are used for quantifying the detector performance. In this framework the sensor coverage, directionality and probabilities of damage occurrence are all accounted for. The effect of cross-correlation among actuator-sensor pairs is then considered by presenting an appropriate model for covariance structure. Applying the genetic algorithm, the global false alarm rate is minimized for a target global detection rate and different levels of correlation. In addition, the receiver-operating characteristic (ROC) is determined to analyze the effect of correlation on the system performance and optimal arrangement. For demonstration of the effect of cross-correlation on damage detection a numerical analysis is carried out using ABAQUS standard. Finally, it is concluded that by increasing the correlation among actuator-sensor pairs, the performance of the SHM system decreases.

Keywords: structural health monitoring; optimal sensor placement; Bayes risk; detection theory; lamb wave

1. Introduction

Structural health monitoring involves with identifying the health state of the mechanical, civil and aerospace structures and is defined as the non-destructive and continuous monitoring of the structures using an array of sensors. In the other words SHM is the process of in-service and real-time monitoring data acquisition for health management of structural system and scheduling maintenance routines (Adams 2007). SHM reduces the maintenance costs because it detects the accumulated damage before reaching to its critical level (Gopalakrishnan *et al.* 2011). The key idea in SHM is to compare data acquired from damaged state to a baseline that can be thought of as the measurements taken when the structures is undamaged. To enhance the performance of the detection process it is required to reduce data dimension using signal processing in order to extract effective features that are representative of the damages (Farrar and Worden 2013).

*Corresponding author, M.Sc., E-mail: fazel@aut.ac.ir

^a Professor, E-mail: hosseini@aut.ac.ir

One of the most critical issues in SHM is the optimal system design in order to assess the state of the structure with a desirable accuracy. Some factors that play rule in system design include transducer arrangement, operational and environmental conditions and type of sensors. For example, it is desirable to place the limited number of actuator/sensors in positions that can maximize the detection performance and minimize the cost. Optimal sensor placement (OSP) approaches are widely used to maximize the detection performance of a SHM system. OSP strategies have also the potential to reduce life cycle costs, risk of false detection and cost of closure and maintenance of structures.

The first famous attempt towards OSP approaches was introduced by Kammer (1991). In his research, the optimal arrangement is determined by minimizing determinant of Fisher information matrix (FIM). FIM denotes the error covariance matrix of the estimated parameters, which reflects the importance of the dynamic information in the measurement responses. Maximizing the determinant of the FIM will maximize a combination of the spatial independence of the target modal partitions and their signal strength in the sensor data. Liu *et al.* (2008) used the modal assurance criterion (MAC) and modal strain energy (MSE) as objective function to determine the optimal location of sensors. Guo *et al.* (2004) obtained an objective function based on the fact that the presence of damage in the structure leads to a change in the stiffness and consequently mode shapes. They used an improved genetic algorithm to find the optimal positions of sensors on a truss structure. Yi *et al.* (2012a) used a modified monkey algorithm to optimally place the sensors on a high-rise building. They also published another work (Yi *et al.* 2012b) and applied a methodology called asynchronous-climb monkey algorithm (AMA) for optimal sensor placement on canton tower in china. These monkey algorithms were demonstrated to be more accurate than binary coding methods (i.e., evolutionary algorithms) in the local and global search capability. Zhou *et al.* (2014) presented a firefly algorithm for sensor placement problem exploiting modal data. Yang (2018) presented a hybrid optimization algorithm using finite element grids updating for sensor placement optimization. He applied the effective independence method in conjunction with a sensor distribution index for improving OSP performance. Azarbajani *et al.* (2008) applied a probabilistic method based on the concept of probability of detection (POD) for optimal sensor placement on a bridge structure. Sun and Büyükoztürk (2015) proposed a discrete optimization using artificial bee colony algorithm for OSP in three structures: a 27 bar Truss Bridge, a 21-storey building at the MIT campus and the 610 m high Canton Tower. Yi *et al.* (2016) used the wolf algorithm for OSP based on a multiaxial modal assurance criterion.

Most of the works in literature have been dedicated to OSP based on modal properties of the structure whereas there have been a few studies in the framework of GWSHM. Lee and Staszewski (2007) studied the effect of sensor-actuator positions on the reliability of damage detection process. They used the local interaction simulation method and experiment to obtain amplitude of wave packages scattered from a rectangular slot with different sizes and fatigue crack. Their study reveals that the best locations for sensors are the areas where the increase in amplitude of wave packets is higher than other regions. In the research done by Gao and Rose (2006), a confident monitoring region is presented for a damage probability distribution. The formula for probability of detection is simply derived from the assumption that the signal strength is proportional to the inverse of the distance between sensor and damage. Das *et al.* (2009) faced the problem of OSP by presenting the certainty region of actuator-sensor pairs. Without consideration of directionality, they minimized the overlap between neighbouring sensors to place sensors in regions with best spatial coverage. Mallardo *et al.* (2012) utilized a probabilistic analysis for optimal placement of piezoelectric sensors for impact localization in a stiffened composite panel.

They introduced a fitness function as a measure of probabilistic error for impact detection and minimized that by genetic algorithm. Thiene *et al.* (2016) proposed an OSP strategy by maximizing the coverage area of sensors in a composite panel. This methodology relies on physical properties of wave propagation and geometrical features of structure. Salmanpour *et al.* (2016) extended the method for delay and sum damage detection algorithm while considering the other physical constraints including line of sight of the sensors, the attenuation due to distance and attenuation due to stiffeners. Similar to the work of Gao and Rose (2006), Coelho *et al.* (2011) presented an OSP method based on the maximum coverage area determined by probability of false alarm for a lug joint and naval structure. Tarhini *et al.* (2018) also exploited the concept of coverage area and determined the optimal piezoelectric sensor locations using mixed integer nonlinear programming. Vanli *et al.* (2012) tried to minimize the maximum probability of non-detection (POND) through their minimax algorithm. Venkat *et al.* (2015) have done a numerical and experimental analysis and demonstrated that the points with high amplitude are best locations for recording signals. Ewald *et al.* (2018) use a similar approach but instead of locating sensors at the highest point, they recommend identification of the area of maximum difference using the blob detection algorithm.

All of the above mentioned guided wave-based OSP strategies define fitness function based on the coverage area and wave amplitude strength over the structure and they are application specific. Flynn and Todd (2010a) introduced a new flexible approach to OSP for GWSHM. They developed the Bayes risk formulation that takes local costs of decisions and a prior probability distribution of damage into account and then derived the optimal detector that minimizes the Bayes risk. They introduced two performance measures, global detection rate (complement of type II error) and global false alarm rate (type I error) as the candidate objective functions and then maximized the former to determine the optimal arrangement. The approach considers both coverage and directionality of the wave packets generated from active piezoelectric sensors in a flexible statistical framework. In addition, it is possible to simultaneously consider the effect of boundaries, prior knowledge of damaged areas, structural features (stiffeners), attenuation of wave and scattering pattern for any kind of damage shape.

In this paper we use the general framework described by Flynn and Todd (2010a) and address the issue of effect of spatial correlation among actuator-sensor pairs on the system performance and optimal arrangement in GWSHM. In SHM systems, deploying densely distributed sensors could monitor the local structural regions with high spatial resolution, which yields to highly correlated measurements. Beside the fact that the existence of measurement correlation provides better local resolution, it seriously degrades the global detection performance if neglected and increases the difficulty of distributed data processing. First fundamentals of the detection theory and Bayesian decision making are presented and applied to the OSP problem. The pitch-catch activation scheme is considered for active sensing process and feature vectors are statistically modeled by multivariate Gaussian probability density function (PDF). Then the relations for mean and covariance structure are modeled in terms of the actuator/sensor placement and the damage position. Afterward the global false alarm rate is minimized for some hypothetical global detection rates with three levels of correlation using genetic algorithm. The spatial maps of local detection rate and local false alarm rate and the ROC curves are obtained and discussed. To verify the effectiveness of the proposed issue in GWSHM a finite element analysis is done using commercial ABAQUS software to simulate the propagation of guided waves in an aluminum plate under healthy and damaged states. Then a damage localization technique is applied on the differenced signals for each optimized sensor arrangement.

2. Theoretical framework

2.1 Bayes risk detector

The Bayesian decision making (damage detection) treats the event probabilities as measures of knowledge or belief. In this way it is possible to assign probabilities to priori knowledge about an event or state (Berger 1980). In OSP problems this state of nature is damage states over the entire regions of structure. Bayes risk or integrated risk is the loss (cost) function averaged over state of nature and feature space. It is computed as the sum of the expected costs of every outcome, which is equal to the cost of each outcome multiplied by the probability of that outcome occurring. In SHM, these outcomes consist of all the possible combinations of predicted (decided) and true damage states of the structure.

Flynn and Todd developed a practical formulation for the Bayes risk by dividing the structure into K spatial regions and considering some logical assumptions such as linearization of cost function and putting emphasis on local costs of decision. For binary damage states each region k takes on two states: the state m_0 as undamaged and the state m_1 as damaged case. In this sense the total Bayes risk is written as (Flynn and Todd 2010)

$$C = \sum_{k=1}^K \sum_{i,j=0}^1 c_{ij}[k] \cdot P(d_{ki}|h_{kj}) \cdot P(h_{kj}) \quad (1)$$

where $c_{ij}[k]$ is the local cost of deciding the damage state m_i when the true state is m_j , $P(h_{kj})$ the probability of the true local damage state, m_j , in region k and $P(d_{ki}|h_{kj})$ the conditional probability of deciding the damage state m_i at region k , d_{ki} , when the true state is m_j . Now one can derive the local binary detector that minimizes the Bayes risk. The Bayes risk can be rewritten as follow

$$C = \sum_{k=1}^K \left(c_{00}[k] \cdot P(d_{k0}|h_{k0}) \cdot P(h_{k0}) + c_{01}[k] \cdot P(d_{k0}|h_{k1}) \cdot P(h_{k1}) + c_{10}[k] \cdot P(d_{k1}|h_{k0}) \cdot P(h_{k0}) + c_{11}[k] \cdot P(d_{k1}|h_{k1}) \cdot P(h_{k1}) \right) \quad (2)$$

The conditional probability $P(d_{ki}|h_{kj})$ is given by Eq. (3).

$$P(d_{ki}|h_{kj}) = \int_{V_{ki}} p(v|h_{kj}) dv \quad (3)$$

where v is the feature vector and V_{ki} is the critical decision region for d_{ki} . In the other hand the conditional probability over d_{k0} is complement of that over d_{k1} (Kay 1998)

$$\int_{V_{k0}} p(v|h_{kj}) dv = 1 - \int_{V_{k1}} p(v|h_{kj}) dv \quad (4)$$

By substituting Eqs. (4) and (3) into Eq. (2) the Bayes risk is

$$C = \sum_{k=1}^K \left(c_{01}[k] \cdot P(h_{k1}) + c_{00}[k] \cdot P(h_{k0}) + \int_{V_{k1}} \left\{ [c_{10} \cdot P(h_{k0}) - c_{00} P(h_{k0})] P(v|h_{k0}) + [c_{11} \cdot P(h_{k1}) - c_{01} P(h_{k1})] P(v|h_{k1}) \right\} dv \right) \quad (5)$$

So, the Bayes risk detector can be stated as “decide m_1 at region k only if the integrand is negative in the other words (Flynn and Todd 2010a)

$$(c_{10} \cdot P(h_{k0}) - c_{00}P(h_{k0}))P(v|h_{k0}) < \dots (c_{11} \cdot P(h_{k1}) - c_{01}P(h_{k1}))P(v|h_{k1}) \quad (6)$$

By assuming that the cost of making correct predictions of each state is less than making incorrect predictions, the detector is (Flynn and Todd 2010a)

$$T[k] = \frac{p(v|h_{k1})}{p(v|h_{k0})} > \frac{(c_{10}[k] - c_{00}[k]) P(h_{k0})}{(c_{01}[k] - c_{11}[k]) P(h_{k1})} \quad (7)$$

For notational simplicity, one can rewrite the cost ratio as (Flynn and Todd 2010a)

$$\gamma[k] = \frac{(c_{10}[k] - c_{00}[k])}{(c_{01}[k] - c_{11}[k])} \quad (8)$$

The cost function in general will be a function of inspection and failure costs. In decision making the cost ratio is called the decision threshold. If the cost ratio is set to one for all regions, then the optimality criteria reduces to the minimum probability of error (Kay 1998). In Bayesian decision making a set of cost ratios must be derived so that they minimize either the total type I or the type II error rate when the other is fixed. Type I error of false positive is the situation in which the state of a structure is identified as damaged while the true state of structure is undamaged which leads to unnecessary inspection and repair of the structure and introduces additional costs. Type II error or false negative occurs when the structure is detected to be healthy when the real state of the structure is damaged and this may result in further damage progression or catastrophic failures.

2.2 Performance measures

For present OSP problem the performance metrics for the detector are considered to be global detection and false alarm rate that quantify the performance of the system. These performance measures are equivalent to the weighted average of correctly detecting a damaged region as damaged and incorrectly detecting an undamaged one as damaged over all damage modes. The global detection and false alarm rate are expressed as (Flynn and Todd 2010a)

$$\bar{P}_D = \sum_{k=1}^K \frac{P(d_{k1}|h_{k1})P(h_{k1})}{\sum_{k=1}^K P(h_{k1})} \quad (9)$$

$$\bar{P}_{FA} = \sum_{k=1}^K \frac{P(d_{k1}|h_{k0})P(h_{k0})}{\sum_{k=1}^K P(h_{k0})} \quad (10)$$

where $P(d_{k1}|h_{k1})$ and $P(d_{k1}|h_{k0})$ are PDF of the detector under alternative and null hypotheses. The optimal set of cost ratios can be determined by fixing one of the two performance criteria and maximizing (or minimizing) the other. This constrained problem is solved using

Lagrange multipliers, that is the optimal set of cost ratios are calculated for optimizing \bar{P}_D or \bar{P}_{FA} for the constraint $\bar{P}_{FA} = \alpha_{FA}$ or $\bar{P}_D = \alpha_D$, respectively. In the other words (Flynn and Todd 2010a)

$$\sum_{k=1}^K p_T(\gamma[k]|h_{k1})P(h_{k1}) - \lambda \sum_{k=1}^K p_T(\gamma[k]|h_{k0})P(h_{k0}) = 0. \quad (11)$$

$$\bar{P}_{FA} - \alpha_{FA} = 0 \quad \text{or} \quad \bar{P}_D - \alpha_D = 0. \quad (12)$$

where p_T is the probability distribution function of the detector, α_{FA} and α_D denote the allowable global false alarm rate and the target global detection rate.

2.3 Detector statistics

The features are representative of real data acquired from experimentation/simulation and affect the damage detection process and optimal arrangement. The desired feature here which is also the most prominent one in GWSHM is the subtraction of damaged and undamaged signals. Other features maybe the difference of signal energies, cross correlation and other statistical measures of two signals in damaged and healthy conditions. To derive the detector one must first obtain the probability distribution of the features and its statistics. For the sake of simplicity, we just consider Gaussian distribution. This assumption is valid for most of SHM problems because the received signals which are inherently random and consist of many ensembles, are averaged for each time bin. The optimal detector for non-Gaussian features can be determined using Monte-Carlo method to numerically integrate the right tail probabilities with some additional complexities. So, the feature vector takes the form of (Flynn and Todd 2010a)

$$v = \begin{cases} N(0, \Sigma_k) , h_{k0} \\ N(\mu_k, \Sigma_k) , h_{k1} \end{cases}. \quad (13)$$

where μ_k and Σ_k are the mean and covariance matrix of the feature for damage mode, k. By substituting the feature PDF into the optimal detector given in Eq. (7) and taking the natural logs from both sides leads to the traditional form of the linear detector (Flynn and Todd 2010a)

$$T^*[k] = v^T (\Sigma_k)^{-1} \mu_k > \gamma^*[k] \quad (14)$$

The new threshold then takes the form (Flynn and Todd 2010a)

$$\gamma^*[k] = \ln(\gamma[k]) + \frac{1}{2} (\mu_k)^T (\Sigma_k)^{-1} (\mu_k) + \ln\left(\frac{P(h_{k0})}{P(h_{k1})}\right). \quad (15)$$

The detector is a now a weighted sum of Gaussian random variables and, as a result, is also Gaussian. By taking expectation and variance of the detector the detector statistics are then (Flynn and Todd 2010a)

$$T^*[k] = \begin{cases} N(0, d^2[k]) \\ N(d^2[k], d^2[k]) \end{cases}. \quad (16)$$

where $d^2[k]$ referred to as the “deflection coefficient” that is a measure of the separation of two Gaussian-distributed variables and defined as (Flynn and Todd 2010a)

$$d^2[k] = \mu_k^T \Sigma_k^{-1} \mu_k. \quad (17)$$

The new Lagrange multiplier $\lambda' = \ln(\gamma[k])$ in Eq. (15) must be solved by constraining one of the performance metrics. After inserting the detector statistics into Eqs. (9) and (10) the two performance metrics are written as (Flynn and Todd 2010a)

$$\bar{P}_{FA} = \sum_{k=1}^K Q \left(\frac{\lambda' + \ln(P(h_{k0})/P(h_{k1})) + 0.5d^2[k]}{\sqrt{d^2[k]}} \right) \frac{P(h_{k0})}{\sum_{k=1}^K P(h_{k0})}. \quad (18)$$

$$\bar{P}_D = \sum_{k=1}^K Q \left(\frac{\lambda' + \ln(P(h_{k0})/P(h_{k1})) - 0.5d^2[k]}{\sqrt{d^2[k]}} \right) \frac{P(h_{k1})}{\sum_{k=1}^K P(h_{k1})}. \quad (19)$$

Here, $Q(\gamma)$ is the right tail probability of a zero-mean, unit-variance, and Gaussian random variable, which can be expressed using the complementary error function, *Erfc*

$$Q(\gamma) = \int_{\gamma}^{\infty} \frac{1}{\sqrt{2\pi}} \exp\left(-\frac{1}{2}t^2\right) dt = \frac{1}{2} \text{Erfc}(\gamma/2). \quad (20)$$

To determine the optimal actuator/sensor arrangement one must first decide whether to maximize global detection rate or minimize global false alarm rate. In this study the global false alarm rate is minimized for fixed global detection rates because of its faster convergence. After that the Lagrange multiplier λ' has to be calculated using Eq. (19) for a fixed global detection rate and an initial value of deflection coefficient for a two-transducer arrangement all over the structure. The spatial distribution of deflection coefficient is obtained for a single pair of transducers which is constructed from one way actuator-sensor path. Note that because the actuation scheme is considered to be only the pitch-catch, there is just one path between two transducers. By substituting the desired global detection rate into the left side of Eq. (19) and the deflection coefficient and damage statistics into the right side of Eq. (19), the Lagrange multiplier λ' can be obtained numerically. Finally, the Lagrange multiplier is substituted into the right side of Eq. (18) to evaluate the global false alarm rate as the fitness function in genetic algorithm.

3. Statistical models of feature vector

Feature statistics plays a key role in SHM applications, particularly the present OSP strategy because it must give reliable information regarding the physics of wave propagation, size and type of damage, environmental conditions and etc. and finally classify the state of the structure. The features translate measurements into decisions regarding the state of the structure or regarding future actions with respect to the structure's operation. This process is been used basically in statistical pattern recognition paradigm (Farrar and Worden 2013). In what follows first the geometric parameters are defined and then the components of feature vector are modeled.

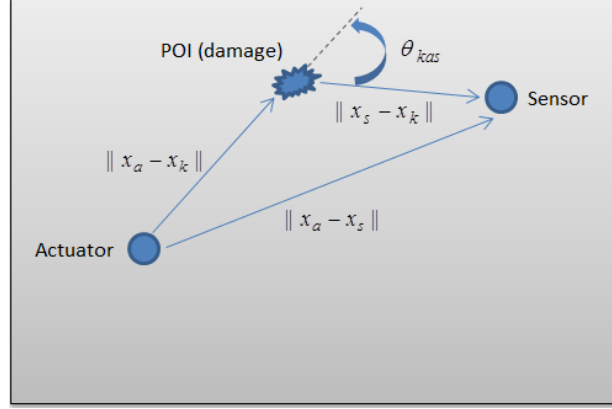


Fig. 1 Distances between actuator-POI-sensor

3.1 Definitions

The length of the features depends on the number of transducers, actuation scheme and discrete regions. We chose pitch catch scheme so with N number of sensors the total actuator-sensor path is $p = C(2, N) = N(N - 1)/2$. For example, the total paths for a sensor network consisting of 5 sensors that serve as both actuator and sensor are $p = C(2, 5) = 10$. So, if the structure is discretized to K regions, the total length of feature vector is Kp . Noted that each region must be small enough to be represented by its centroids. These centroids are called points of interest (POI).

Spatial coordinates of actuator, sensor and POI are denoted as vectors x_a , x_s and x_k . The locations of actuator, POI and sensor and their distances are depicted in Fig. 1. In addition, the angle created between actuator-POI-sensor is denoted by θ_{kas} . Note that in GWSHM a wave propagation path is referred to the path from actuator to POI and from POI to sensor. The $\|()\|$ operator denotes the Euclidean distance between two vectors

$$\|r_1 - r_2\| = \sqrt{(r_1 - r_2) \cdot (r_1 - r_2)} \quad (21)$$

where r_1 and r_2 are two arbitrary vectors in 2D space and dot indicates the inner product between two vectors. The angle between two vectors is determined as follow

$$\theta = \text{Arc cos} \left(\frac{r_1 \cdot r_2}{\|r_1\| \cdot \|r_2\|} \right) \quad (22)$$

3.2 Mean structure

The mean vector is expressed as follow (Flynn and Todd 2010a)

$$\mu_k[p] = A_e \left(\frac{\eta}{\eta + \sqrt{r_{ka}}} \right) S(\theta_{kas}) \left(\frac{\eta}{\eta + \sqrt{r_{ks}}} \right). \quad (23)$$

The term A_e accounts for the overall actuation and sensing system efficiency i.e., the amplitude of the initial driving signal as well as the transducer efficiency of the actuator and sensor.

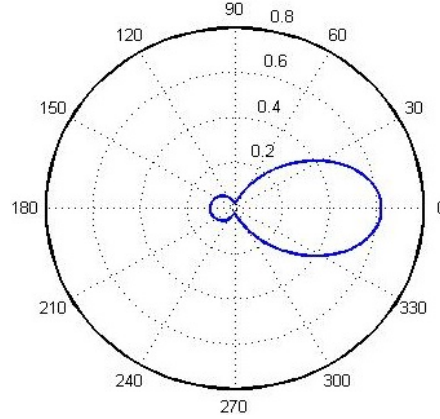


Fig. 2 Far field scattering

The second is the beam spread function that captures the amplitude reduction of the planar point-source wave and follows the physics of wave propagation. In the other words, this function is inversely proportional to the square root of distance between transducer and POI. The parameter η approximates the finite near-source behaviour of the propagating waves. The scattering term $S(\theta_{kas})$ used to model the change in the feature amplitude due to the relative positioning of the POI with respect to the actuator and sensor. To model the $S(\theta_{kas})$, it is assumed that the defect is a symmetric scatterer and the dominant mode of far-field scattering is longitudinal. The scattering term is presented as (Flynn and Todd 2010a)

$$S(\theta_{kas}) = 0.18 + 0.19 \cos(\theta_{kas}) + 0.17 \cos(2\theta_{kas}) + 0.068 \cos(3\theta_{kas}) + 0.014 \cos(4\theta_{kas}) \quad (24)$$

where θ_{kas} is the angle between the vector formed by the actuator and POI and the vector formed by the POI and sensor. This model is a specific form of the far-field scattering presented in publications (Diligent *et al.* 2002 and Grahn 2003) that emphasizes on the forward direction. This analytic model is verified by finite element analysis and experiments in the research of Diligent *et al.* (2002). The polar plot of this model is shown in Fig. 2. As can be seen the main lobe of the symmetric lamb wave mode, S_0 , is in the forward direction.

It is worth mentioning that the scattering term can be determined from theoretical and/or numerical analysis and experimentation for any specific application. For example, for defects with different shapes and sizes, the wave scatters in different directions can be determined using FEM and modeled in terms of the angle between incident and scatter angles. In addition, if there are some structural features such as stiffeners perpendicular to the propagation path, one can also derive a scattering term by considering the transmission and reflection of incident waves propagate through the stiffener.

3.3 Covariance structure

Of interest in this material is to analyze the effect of cross correlation among actuator-sensor pairs on the performance of GWSHM system. In the other words we have to present a statistical model for non-diagonal elements of covariance matrix. The statistical model for the mean vector

and diagonal elements of covariance matrix were considered as the same one presented by Flynn and Todd (2010b). It is worth mentioning that the covariance matrix of a multivariate PDF in a GWSHM system contains information regarding to the noise processes. The noise processes may arise from changes in temperature or boundary conditions and sensor electrical/mechanical noise. In the next two subsections the statistical model for diagonal and non-diagonal elements of covariance matrix are presented.

3.3.1 Diagonal elements of covariance matrix

The diagonal elements of the covariance matrix are scaled linearly by the total propagation path and take the form (Flynn and Todd 2010a)

$$\sigma_k[p] = (r_{ka} + r_{kb})\phi_p + \sigma_m. \quad (25)$$

Here the parameter σ_m can be thought of as the ambient noise that is independent of sensor arrangement and ϕ_p is a scaling parameter.

3.3.2 Non-diagonal elements of covariance matrix

The spatial correlation amongst actuator-sensor pairs in any sensor network system is important because two sensors in close proximity have a strong spatial correlation and capture almost the same data and consequently degrades the performance of the systems (Liu 2007 and Kim *et al.* 2009). For example, in cognitive radio networks, for a desired detection probability and constant signal to noise ratio (SNR), the false alarm probability of the energy detector increases as cross correlation among multiple antennas increases (Kim *et al.* 2009). The same analysis and conclusions are presented by Shbat and Tuzlukov (2013) for assessing the performance of the generalized detector in spectrum sensing. It is proved that an exponential model can capture the dependence of correlation coefficient on the antenna placement.

So back to GWSHM applications, by taking this effect into account one can avoid overestimating the system performance and use a few numbers of sensors that reduces the cost of SHM system design and the dimension of data. It is evident that the correlation between two neighboring sensors is higher than correlation between two sensors that are far apart. In the other hand the non-diagonal elements of the covariance matrix are obtained by multiplying variances of two variables by the correlation coefficient. So, it is reasonable to model the spatial correlation in terms of sum of a second order polynomial and an exponential function decreasing along the propagation path. In the other words the covariance structure for pairs sharing one actuator can be modeled as below

$$\Sigma_{ij} = b_1 + b_2(r_{ka} + r_{s_i s_j}) + b_3(r_{ka} + r_{s_i s_j})^2 + b_4 \exp(-b_5(r_{ka} + r_{s_i s_j})) \quad (26)$$

where r_{ka} and $r_{s_i s_j}$ are distance from actuator to the POI and the distance between two correlating sensors; b_1 to b_5 are model parameters. For the other pairs the covariance structure is written as

$$\Sigma_{ij} = b_1 + b_2(r_{ka} + r_{s_i s_j}) + b_3(r_{ka} + r_{s_i s_j})^2 + b_4 \exp(-b_5(\Delta r_{kas} + r_{s_i s_j})) \quad (27)$$

where Δr_{kas} is the distance between actuators of two different pairs. It is noted that the exponential term accounts for inverse relation between correlation and spatial positions of

measurement points (Kim *et al.* 2009 and Shbat and Tuzlukov 2013). The term b_1 is independent of transducer placement and used to control the levels of cross-correlation amongst actuator-sensor pairs. It is worth mentioning that determining the covariance structure using experimentation leads to cost insufficiency since it needs many sensors to be installed on a structure.

4. Results

In this section the OSP approach is demonstrated through hypothetical scenarios. We seek to optimally place 5 sensors on a rectangular plate so the total number of paths is $p = 10$. The $62 \times 59 \text{ cm}$ plate is divided into discrete regions of size 1 cm^2 . The model parameters are set as follow

$$\eta = 5, A_E = 15, \phi_p = 0.03, \sigma_m = 2, b_2 = 0.09, b_3 = 0.03, b_4 = 0.1, b_5 = 2 \quad (28)$$

To show the effect of cross correlation among sensors on the performance and optimal arrangement we minimized the global false alarm rate for a number of global detection rate values and different correlation levels (i.e., different b_1 values). Fig. 3 shows the spatial map of deflection coefficient for an actuator-sensor pair. After evaluating λ' for each scenario the global false alarm rate (fitness function) in Eq. (18) is minimized to determine the optimal sensor locations. Note that in real applications the parameters in Eq. (28) are case dependent and can be evaluated using a nonlinear-regression on data acquired from a dense array of transducers when the structure is undamaged. The signals are recorded for as many as possible sets of three transducers with different locations. For each set with two paths a bivariate PDF is considered and its statistics are estimated by sample mean and covariance of the received signals. By repeating this and recording the values of mean covariance elements, a nonlinear regression is applied to fit the data to Eqs. (27)-(29).

The authors selected the genetic algorithm to search for optimal sensor locations because it is quite easy to implement and is appropriate for searching in multidimensional discrete space. In

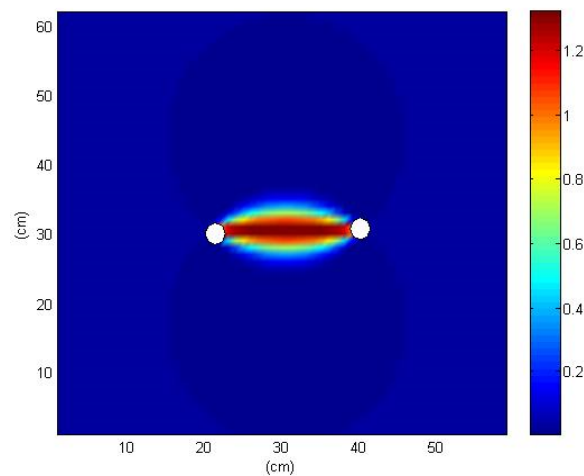


Fig. 3 Spatial map of deflection coefficient for two-transducer arrangement in pitch-catch scheme

genetic algorithm coding, every individual (sensor locations) is expressed by 8-bit string of 0 s and 1 s. For the population size of 40 and mutation rate of 0.015 the program starts with an initial population and continues iteratively by applying one-point cross-over and forced mutation until the global false alarm rate converges. For avoiding local optimum one can increase the population size and mutation rate but in the expense of slower convergence. So there have to be a trade-off between accuracy and convergence. Note that the global false alarm is chosen as fitness function because its convergence found to be faster than the case in which global detection is maximized.

4.1 The case of uniform damage rate

In this case the prior probabilities of damage event over the entire structure are assumed uniform. After inserting the PDF of detector in the performance measures, the global false alarm rate is minimized for a fixed detection rate of $P_D = 0.95$. The map of local detection and false alarm rates for uniform distribution of damage probability and different correlation levels $b_1 = 0.2, 0.4, 0.7$ are shown in Figs. 4-6. The resulting global false alarm rates are $\bar{P}_{FA} = 0.047, 0.095, 0.112$.

First of all, it can be inferred from Fig. 4 that the blind regions on the plate which cannot be detected by the network of optimized sensor arrangements are regions far from the direct line of sight between actuator-sensor paths. For instance, three regions at the corners of plate in the map of local detection rate in Fig. 4 which are identified by blue color are blind regions in a detection process. Therefore, one can conclude that for a structure with equal possibility of damage occurrence all over the structural regions, the optimal sensor arrangement is expected to be the one that can cover/monitor most of the regions. The map of local false alarm rates in Fig. 4 indicates that when the sensors are placed at the edges of plate so that the network covers most areas, the probability of falsely detecting the damage in these regions is the least. Secondly by comparing Figs. 4-6 it can be seen that by increasing the cross-correlation among sensors the global false alarm increases which is equivalent to lower detectability of optimized sensor arrangement. In the other words the more actuator-sensors pairs are correlated in the sensor network the more missed-detected blind regions are present on the structure. Despite that in Figs. 5 and 6 the local detection rates are increased in some regions, the quality of coverage is diminished and global detectability

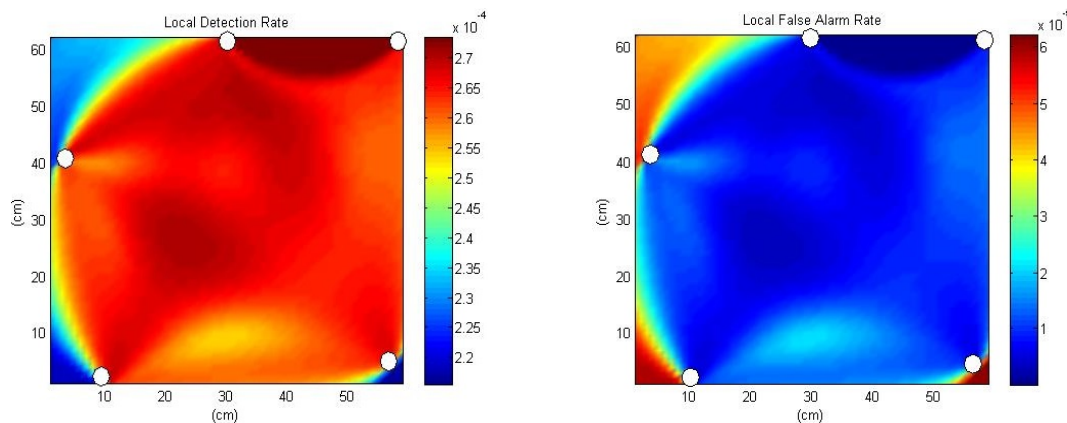


Fig. 4 Local detection (left) and false alarm rate (right) with five-sensor optimal arrangement for a fixed global detection rate of $P_D = 0.95$ and correlation level $b_1 = 0.2$

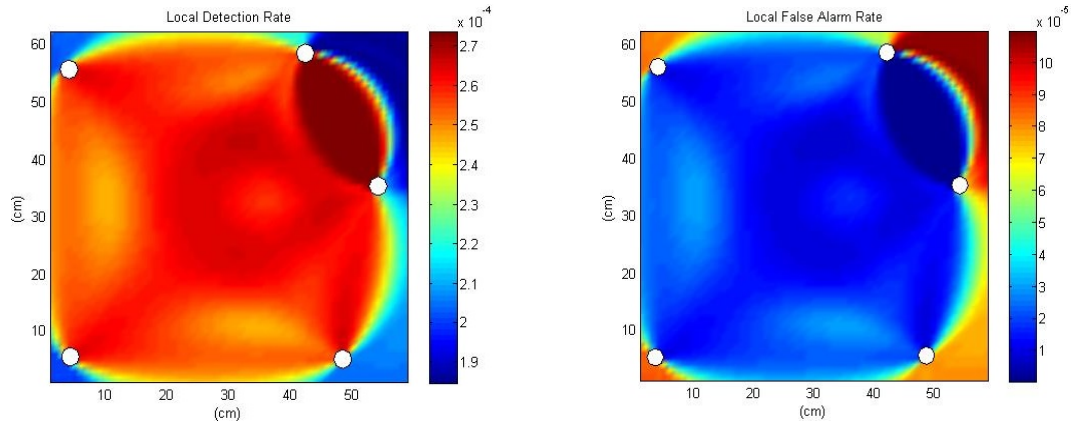


Fig. 5 Local detection (left) and false alarm rate (right) with five-sensor optimal arrangement for a fixed global detection rate of $P_D = 0.95$ and correlation level $b_1 = 0.4$

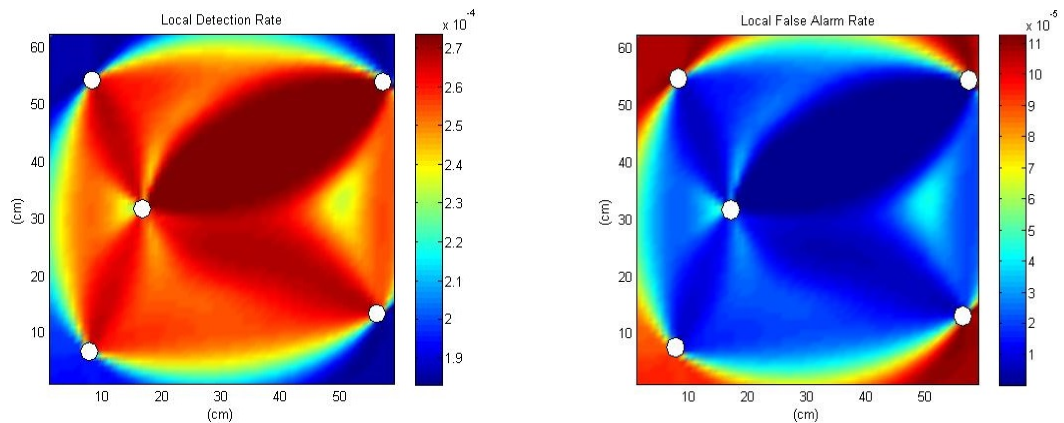


Fig. 6 Local detection (left) and false alarm rate (right) with five-sensor optimal arrangement for a fixed global detection rate of $P_D = 0.95$ and correlation level $b_1 = 0.7$

is reduced for highly correlated pairs. This increases the local probability of detection in areas close to sensors at the expense of lower coverage. It is also noted that the fact of “high detectability in direct line of sight” is more apparent in Fig. 6.

4.2 The case of non-uniform damage rate

In this section the optimal positions of sensor/actuator pairs are obtained for non-uniform damage distributions. In real world applications in the field of civil, mechanical and aerospace engineering, complex structures are constructed from two or more parts joined by using techniques such as welding, riveting and bolt fasteners. In this case the damage probabilities are non-uniform because the possible damages initiate at regions around joint connections (regions with high stress concentration). As can be seen schematically in Fig. 7, three rows of rivets joined two plate-like structures.

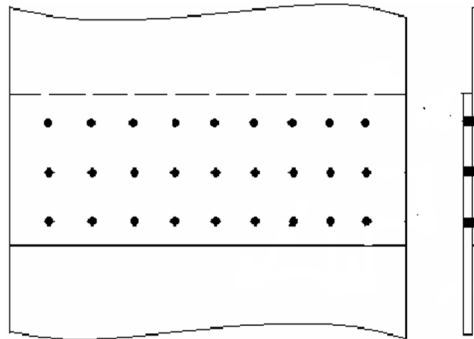


Fig. 7 Riveted joints connecting two panels

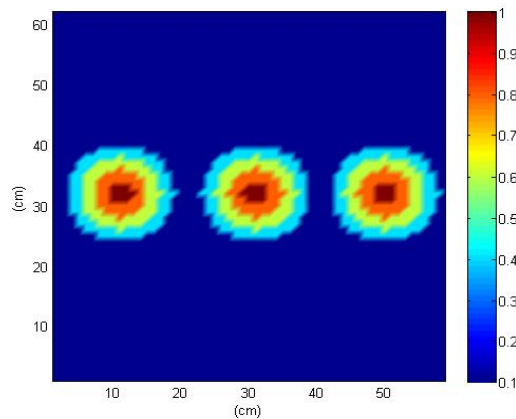


Fig. 8 Non-uniform damage distributions over the plate with three riveted holes

In order to understand the effect of damage probability distribution on OSP problem we consider three holes on the plate to account for rivet locations. Fig. 8 shows a typical spatial map of non-uniform damage probabilities over the structural regions. As depicted the regions around rivet holes have a high probability of damage occurrence.

Now the procedure in the 4.1 section is repeated and optimal arrangements is obtained using the genetic algorithm. For the global detection rate of $P_D = 0.95$ the global false alarm rate is minimized to obtain the optimal arrangement. This is repeated for three levels of correlation levels $b_1 = 0.2, 0.4, 0.7$. The local detection rates and false alarm rates are depicted in Figs. 9-11. The resulting global false alarm rates are $\bar{P}_{FA} = 0.044, 0.0937, 0.088$.

According to these Figures the most apparent point is that the algorithm provides the optimal arrangement so that the detection rate is high in regions around rivet holes. Similar to the case of uniform damage distribution, the regions at the corners of the plate are blind regions and have the least probability of detection which can be easily observed in Fig. 9. The map of local false alarm rate in Fig. 9 indicates that around the third hole, the false alarm rate is maximum which is the result of using pitch-catch-scheme. That is the regions neighboring the direct line of sight of more actuator-sensor paths have less false alarm rate and better detectability. For instance, the regions around the last actuator-sensor path have less probability of detection than that of for example the

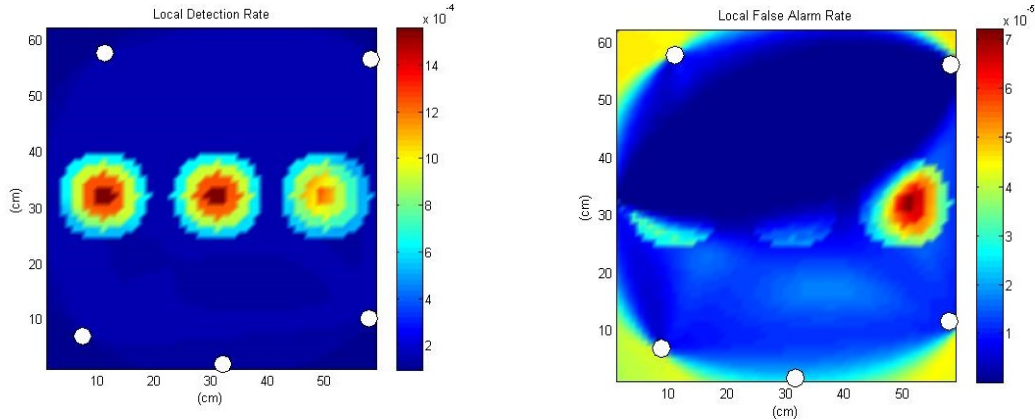


Fig. 9 Local detection (left) and false alarm rate (right) with five-sensor optimal arrangement for a fixed global detection rate of $P_D = 0.95$ and correlation level $b_1 = 0.2$

first path which can also be covered by other adjacent paths. This can be overcome by considering the pulse-echo mode of actuation but at the expense of higher cost, higher data dimension and numerical costs. It can be inferred from Figs. 10 and 11 that the optimal locations are close to high damage rate regions as expected. This is the procedure that is been used in practical SHM applications. Similar to the uniform damage case, high correlation amongst pairs results in poor system performance and less coverage over structural regions. The negative effect of cross-correlation is more drastic in this case since it leaves more areas to be miss-detected which is clear in the maps of local false alarm rate in Figs. 10 and 11. So, in the sensor networks with highly correlated arrangements there are more regions to be missed during the damage detection process.

4.3 Receiver operating characteristics (ROC) curves

To Figure out the effect of cross correlation on the system performance quantitatively we plot the global detection rate versus the global false alarm rate for increasing levels of correlation

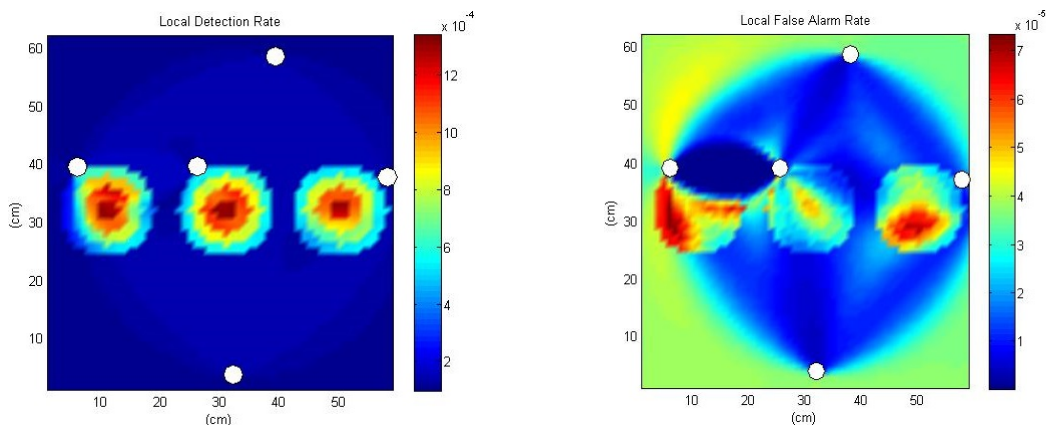


Fig. 10 Local detection (left) and false alarm rate (right) with five-sensor optimal arrangement for a fixed global detection rate of $P_D = 0.95$ and correlation level $b_1 = 0.4$

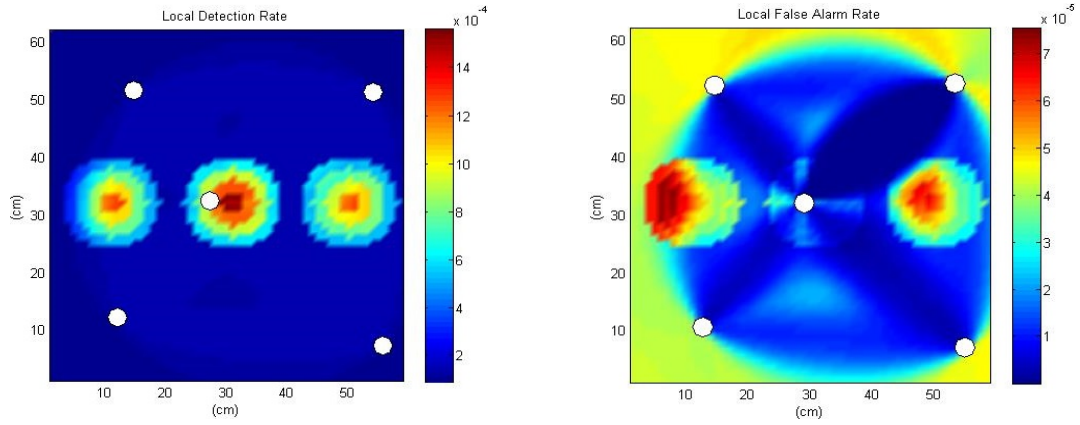


Fig. 11 Local detection (left) and false alarm rate (right) with five-sensor optimal arrangement for a fixed global detection rate of $P_D = 0.95$ and correlation level $b_1 = 0.7$

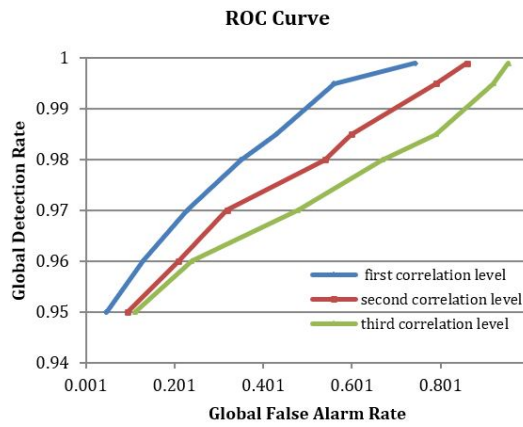


Fig. 12 ROC curve for different levels of correlation for uniform damage distributions

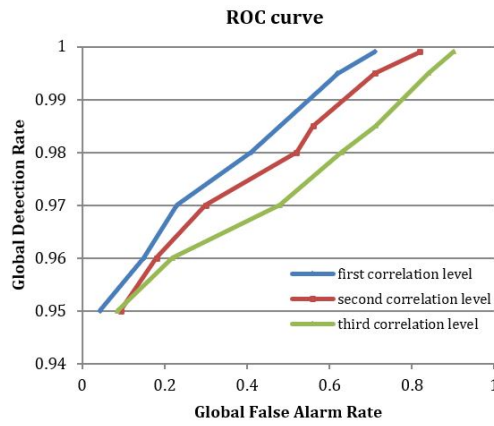


Fig. 13 ROC curve for different levels of correlation for non-uniform damage distributions

(different values of b_1). First, second and third correlation levels are related the values $b_1 = 0.2, 0.4, 0.7$. This can be thought of as global form of well-known Receiver Operating Characteristic (ROC) curves. After running program for 21 hypothetical scenarios, ROC curves for both damage rate cases are obtained and shown in Figs. 12 and 13. As can be seen by increasing the correlation among pairs the performance of the SHM system decreases since the coverage over the structure is diminished. This fact has been mentioned by Flynn and Todd (2010a, b) and has been quantitatively shown in communication systems (Kim *et al.* 2009 and Shbat and Tuzlukov 2013). In the other words for a desired global detection rate which is specified by user, the probability of which the SHM system falsely detects the structural regions as damaged, is increased.

5. Verification of proposed method

5.1 Numerical analysis

To verify the negative effect of cross-correlation on the damage detection a numerical analysis using FEM is carried out for the optimal arrangement obtained from the case of uniform damage probability. The guided wave propagation in an aluminum plate is simulated using commercial software ABAQUS/Explicit. The material properties of $62 \times 59 \times 0.1$ cm aluminum plate are: density $\rho = 2700$ kg/m³, Young modulus $E = 70$ Gpa, poisson's ratio $\nu = 0.33$. The excitation signal is 5 cycle Hanning windowed sinusoid with central frequency of 100 kHz. At this frequency the first antisymmetric mode, A₀, dominates the first symmetric mode, S₀. In GWSHM it is proved that modulation of signals with 5 cycles reduces the frequency band and dispersion behavior and consequently increases the signal energy or (SNR). The excitation signal and its Fourier spectrum are shown in Fig. 14.

To achieve the good spatial and temporal resolution it is recommended that the element size and integration time step must meet the conditions below (Alem *et al.* 2016)

$$\Delta t < \frac{1}{20f_c}, \quad L_{\min} \leq \frac{\lambda}{10} \quad (29)$$

where f_c is the excitation frequency and λ is the wavelength of the desired lamb mode.

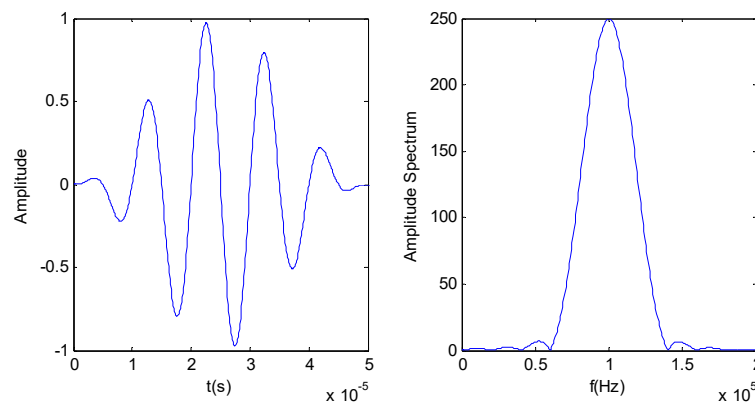


Fig. 14 A 5 cycle tone burst signal and its frequency response

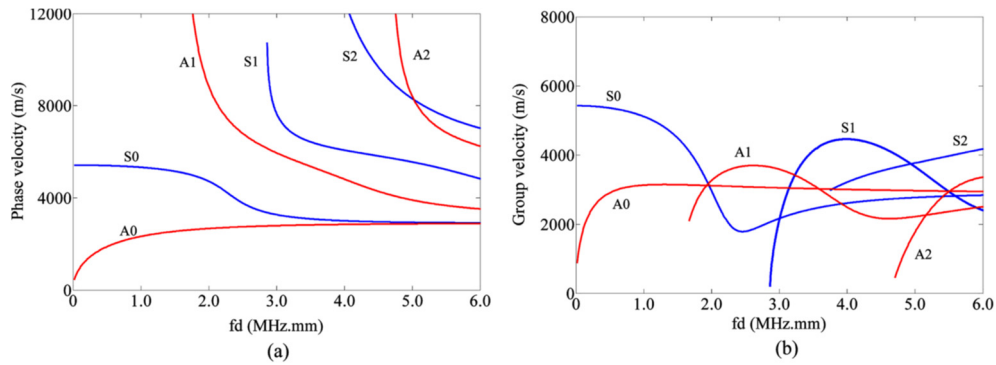


Fig. 15 Dispersion curve of lamb modes for aluminium plate (a) phase velocity; (b) group velocity (Liu *et al.* 2012)

According to the Rayleigh- Lamb dispersion curves in Fig. 15, for center frequency $f_c = 100 \text{ kHz}$ the phase velocity is almost $v_p \approx 1500 \text{ m/s}$, and the wavelength of A0 mode is calculated as $\lambda_{p_{min}}$. Therefore, the element size and time step for the ABAQUS solver must be less than 1.5 mm and 0.5 microseconds respectively. In this study we set the element size and time step to be 1 mm and 0.1 microseconds respectively. To reduce the computational cost, the ABAQUS/EXPLICIT is utilized so that instead of modeling the PZT elements, a nodal force in the thickness direction is applied on the node corresponding to the location of actuator and nodal displacements in the z direction, w , is recorded at sensor locations. The capability of this simplification in fault detection is demonstrated by Bagheri *et al.* (2013). In addition, a continuum

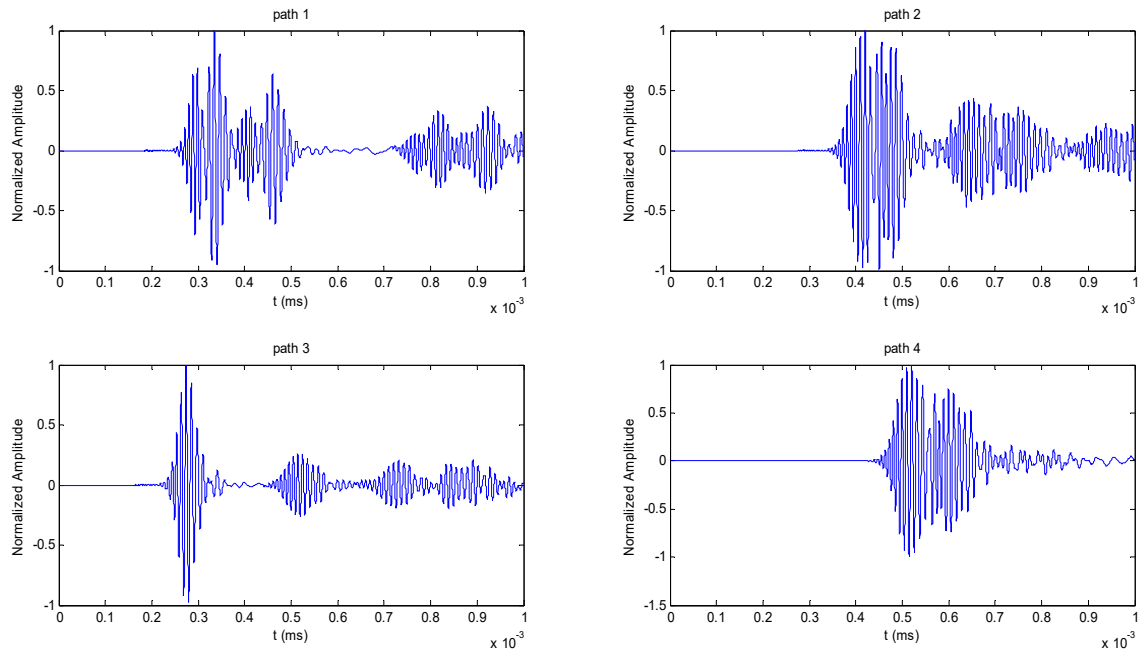


Fig. 16 Signal recorded from path 1-4 in undamaged plate

shell element is used to further decrease the runtime. Sharif-Khodaei and Aliabadi (2014) demonstrated that choosing shell elements can efficiently excite and capture the propagation of fundamental lamb modes.

After setting up the model in ABAQUS for each optimal arrangement, the guided wave packets are recorded for 10 actuator-sensor pairs. An example of the received waveform for optimal arrangement obtained from correlation level $b_1 = 0.2$ in undamaged plate is depicted in Fig. 16. The first wave packet is incident A0 mode and the others are boundary reflections. The presence of strong boundary reflections in received signals which is due to placement of sensors at the plate edges, are automatically removed by differencing signals received in damaged and healthy states.

A through-thickness hole with the diameter of 40 mm is considered as damage. The hole location and its corresponding element distribution is shown in Fig. 17. Computations in ABAQUS are based on Lagrangian scheme so that the elements are attached to material and deform with respect to its mechanical properties. Therefore, the regions around the hole should be discretized in a smooth pattern to efficiently simulate the propagation of guided waves. The element sizes for partitions around the hole are less than 0.9 mm. The total number of 268490 elements is created in the model. Snapshots of the propagation of wave in the damaged plate are

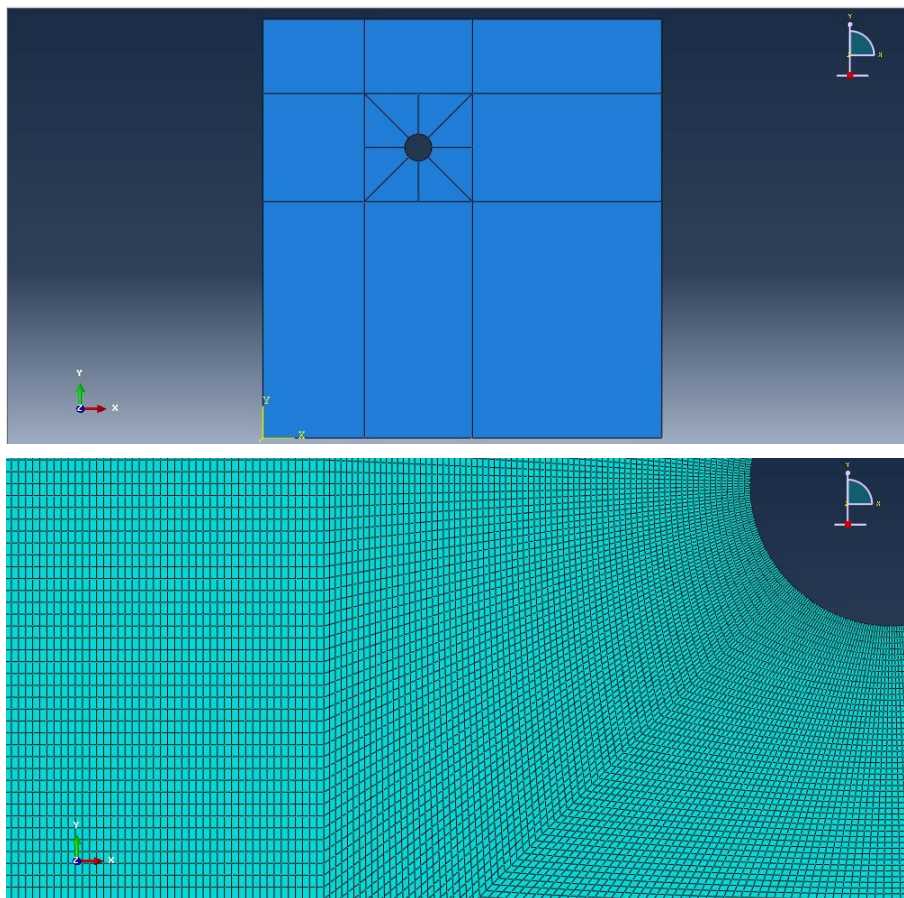


Fig. 17 Position of the through-thickness hole

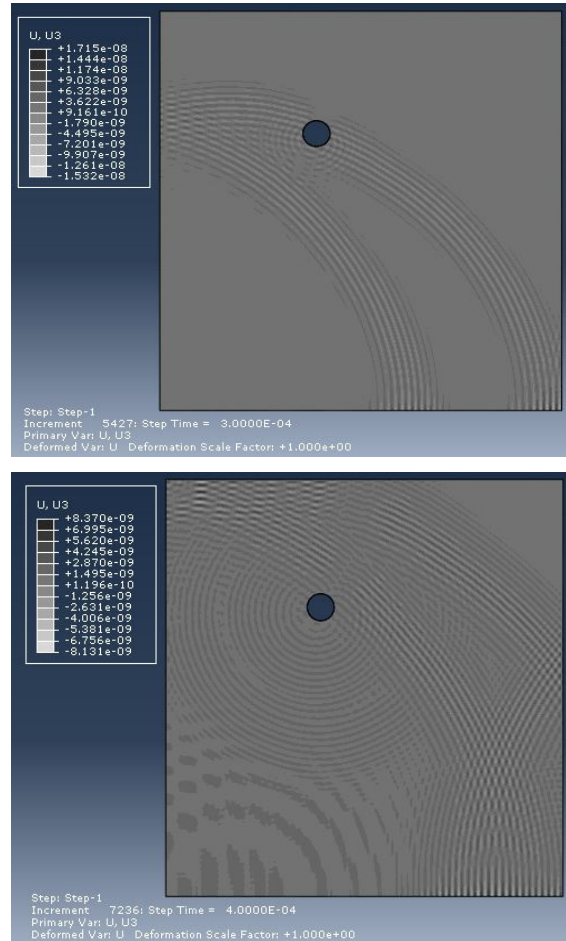


Fig. 18 Wave propagation in presence of a through-thickness hole

depicted in Fig. 18. An example of the recorded signal for path 8 in which sensor 2 acts as actuator and sensor 3 is receiver is illustrated in Fig. 19. First and second wave packets are incident A0 mode and its boundary reflection and the third component is direct wave scattered from the through-thickness hole. Visibility of damage scattered wave is dependent on existence of the damage in direct line of sight from actuator to sensor.

5.2 Damage detection strategy

In GWSHM the detection process is generally based on the comparison of signals acquired in healthy and damaged states. Accordingly, the feature vector is constructed by subtracting the waveforms of damaged state from those of intact structure. After evaluating the feature vector for all actuator-sensor pairs for each optimal sensor arrangement, the well-known delay-and-sum (DAS) beamforming/imaging can be applied to locate the position (Michaels and Michaels 2007, Michaels *et al.* 2009 and Hall *et al.* 2014). DAS method which is also called ellipse method exploits the time of flight (TOF) of the differenced signals. The image pixel at each point on the

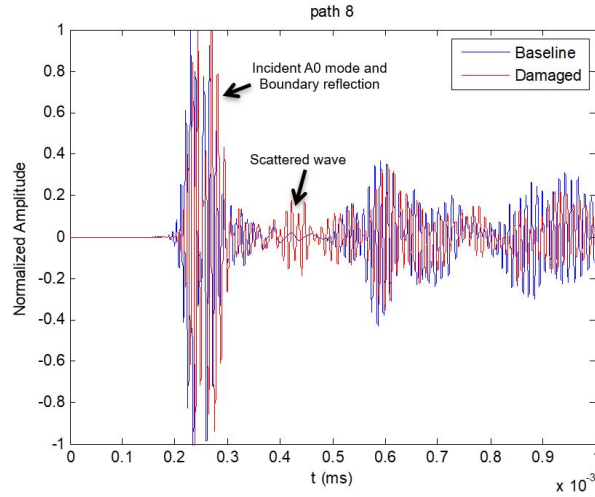


Fig. 19 Received waveforms for path 8 and the case with correlation level $b_1 = 0.2$

plat is evaluated as follow (Michaels and Michaels 2007)

$$I(x, y) = \frac{1}{P} \sum_{i=1}^P |d_i(\tau_i(x, y))|^2 \quad (30)$$

where P is the number of actuator-sensor pairs, d is the feature or differenced signal and τ_i stands for the time of arrival (TOA) of the scattered wave for i^{th} transducer pair.

It is found that scaling the image removes multiple peaks other than the peak related to the damage. Therefore, to improve the image resolution the pixel value is scaled as

$$I'(x, y) = \frac{I(x, y) - \mu_d}{\sigma_d} \quad (31)$$

where μ_d and σ_d are set to be mean and variance of the differenced signal for each propagation path, $d_i(\tau_i(x, y))$.

For pair i the TOA is determined from the distances between actuator, damage (pixel point) and sensor

$$\tau_i(x, y) = \frac{L_{AD} + L_{DS}}{V} \quad (32)$$

where L_{AD} and L_{DS} are the distance from actuator to damage and from damage to sensor. V is the group velocity of the A0 mode and it is assumed to be constant after reflection from damage. The different paths are shown in Fig. 20 schematically. Note that it is assumed that the wave velocity before and after passing through the hole is identical.

5.2 Results of damage detection

We applied the delay and sum algorithm to locate the position of through-thickness hole for three optimized arrangements. Fig. 21 shows the image generated by standard DAS beamforming

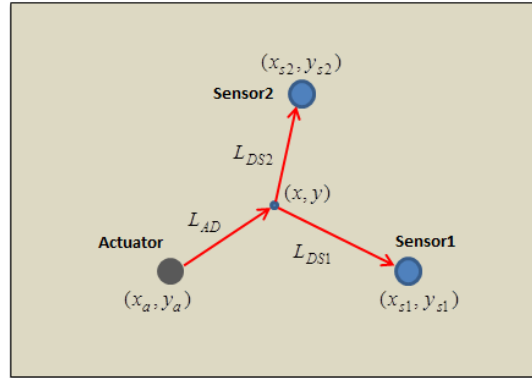


Fig. 20 Propagation paths from an actuator to damage to sensors

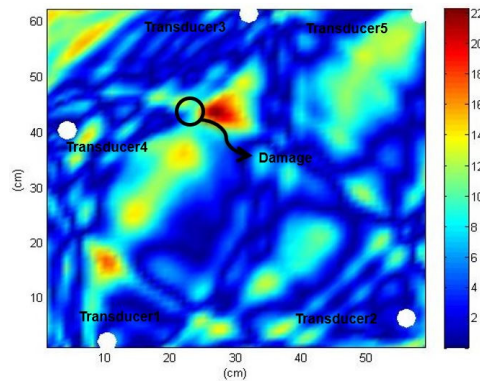


Fig. 21 Delay and sum imaging result with optimal arrangement for global detection rate of $P_D = 0.95$ and correlation level $b_1 = 0.2$

for the optimized arrangement in the first case with the global detection rate of $P_D = 0.95$ and correlation level $b_1 = 0.2$. The current sensor network locates the damage with an acceptable accuracy. The discrepancy between the estimated and true damage position is because the transducers are arranged at plate edges to maximize the coverage and probability of detection for all regions equally. Generally, a transducer arrangement which surrounds the damage region gives the best detection result but in real applications in which there is a constraint regarding the number of sensors and hardware installations, it misses to monitor regions outside the sensor network.

For the second case which has higher correlation level of $b_1 = 0.4$ the result of DAS beamforming is shown in Fig. 22. In this case the damage detection is almost acceptable and the error is less than 5 cm. Besides other major peaks are decreased in the respective image it's accuracy in less than the first case with lower correlated pairs.

For the optimized arrangement with the highest correlation level of $b_1 = 0.7$, the result of damage imaging is illustrated in Fig. 23. Since the damage is surrounded by transducer 3, transducer 4 and transducer 5 and the corresponding pairs have more shares in the image pixel values there is a peak close to the exact damage position. It can also be seen that there is another peak farther from the damage location. So, it is concluded that this transducer arrangement misses

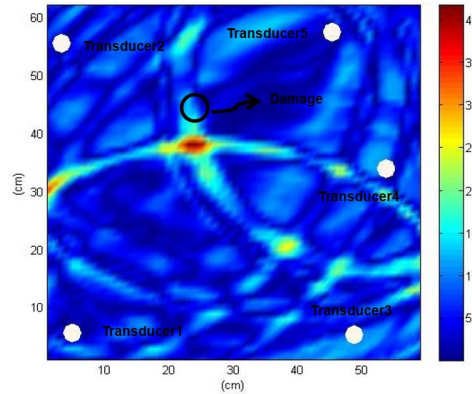


Fig. 22 Delay and sum imaging result with optimal arrangement for global detection rate of $P_D = 0.95$ and correlation level $b_1 = 0.4$

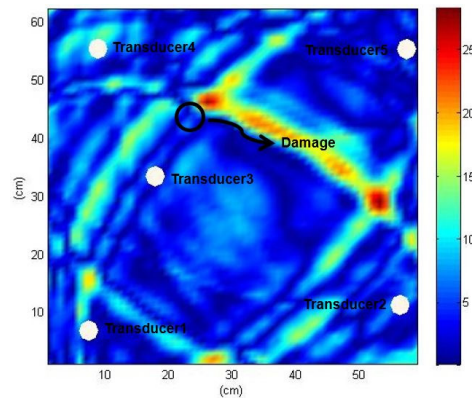


Fig. 23 Delay and sum imaging result with optimal arrangement for global detection rate of $P_D = 0.95$ and correlation level $b_1 = 0.7$

to effectively locate the position of damage and increases the false alarm in inspection of the structure.

6. Conclusions

This paper is devoted to study the sensor placement optimization in GWSHM systems. This problem is tackled using a flexible strategy within a detection theory and a Bayes risk framework so that the physical and geometrical features of structure and damage are accounted for. We minimized the global false alarm rate for a fixed global detection rate using genetic algorithm and determined the optimal arrangement for different scenarios. In particular, the effect of cross-correlation between pairs on performance of the system is taken into account. Spatial maps of local detection rate show that for a targeted global detection rate by increasing the cross correlation among actuator-sensor pairs, the global false alarm rate is increased and system performance is degraded. Considering spatial correlation among features provides more real system performance and meets the SHM system demands such as reducing cost, increasing probability of detection. To

quantify the effect of cross correlation on the system performance the so-called ROC curves are obtained for uniform and non-uniform damage rates. Regarding the ROC curves one can generally say that increasing the sensor correlation would lead to a decrease in performance of the SHM system in terms of its detectability. Finally, the applicability and effectiveness of the optimization results are tested using FEM for an aluminum plate. Results obtained from delay and sum beamforming shows that the accuracy of damage localization is generally weakened in the transducer arrangement with highly correlated pairs. In addition, it is concluded that using spars array of sensor for health monitoring of structures increases the coverage but it would degrade the accuracy of damage localization.

References

- Adams, D.E. (2007), *Health Monitoring of Structural Materials and Components*, John Wiley & Sons Ltd, The Atrium, Southern Gate, Chichester, West Sussex PO19 8SQ, England.
- Alem, B., Abedian, A. and Nasrollahi-Nasab, K. (2016), "Reference-free damage identification in plate-like structures using Lamb-wave propagation with embedded piezoelectric sensors", *J. Aerosp. Eng.*, **29**(6), 04016062. [https://doi.org/10.1061/\(ASCE\)AS.1943-5525.0000646](https://doi.org/10.1061/(ASCE)AS.1943-5525.0000646)
- Azarbayejani, M., El-Osery, A.I., Choi, K.K. and Taha, M.R. (2008), "A probabilistic approach for optimal sensor allocation in structural health monitoring", *Smart Mater. Struct.*, **17**(5), 1-11. <https://doi.org/10.1088/0964-1726/17/5/055019>
- Bagheri, A., Li, K. and Rizzo, P. (2013), "Reference-free damage detection by means of wavelet transform and empirical mode decomposition applied to Lamb waves", *J. Intell. Mater. Syst. Struct.*, **24**(2), 194-208. <https://doi.org/10.1177/1045389X12460433>
- Berger, J.O. (1980), *Statistical Decision theory and Bayesian Analysis*, Springer-Verlag, New York, USA.
- Coelho, C.K., Kim, S.B. and Chattopadhyay, A. (2011), "Optimal sensor placement for active guided wave interrogation of complex metallic components", *Proceedings of Sensors and Smart Structures Technologies for Civil, Mechanical, and Aerospace Systems*, Volume 7981, San Diego, CA, USA, March. <https://doi.org/10.1117/12.880288>
- Das, S., Chattopadhyay, A. and Zhou, X. (2009), "Acoustic based structural health monitoring for composites using optimal sensor placement: analysis and experiments", *J. Reinf. Plastics Compos.*, **28**(1), 83-97. <https://doi.org/10.1177/0731684407084099>
- Diligent, O., Grahn, T., Bostrom, A., Cawley, P. and Lowe, M.J.S. (2002), "The low-frequency reflection and scattering of the S_0 Lamb mode from a circular through-thickness hole in a plate: Finite Element, analytical and experimental studies", *J. Acoust. Soc. Am.*, **112**(6), 2589-2601. <https://doi.org/10.1121/1.1512292>
- Ewald, V., Groves, R.M. and Benedictus, R. (2018), "Transducer placement option of lamb wave SHM system for hotspot damage monitoring", *Aerospace*, **5**(2), 1-17. <https://doi.org/10.3390/aerospace5020039>
- Farrar, C.R. and Worden, K. (2013), *Structural health monitoring: a machine learning perspective*, John Wiley & Sons Ltd., The Atrium, Southern Gate, Chichester, West Sussex PO19 8SQ, England.
- Flynn, E.B. and Todd, M.D. (2010a), "A Bayesian approach to optimal sensor placement for structural health monitoring with application to active sensing", *Mech. Syst. Signal Process.*, **24**(4), 891-903. <https://doi.org/10.1016/j.ymsp.2009.09.003>
- Flynn, E.B. and Todd, M.D. (2010b), "Optimal Placement of Piezoelectric Actuators and Sensors for Detecting Damage in Plate Structures", *J. Intell. Mater. Syst. Struct.*, **21**(3), 265-274. <https://doi.org/10.1177/1045389X09338080>
- Gao, H. and Rose, J.L. (2006), "Ultrasonic sensor placement optimization in structural health monitoring using evolutionary strategy", *AIP Conference Proceedings*, **820**(1), 1687-1693. <https://doi.org/10.1063/1.2184724>
- Gopalakrishnan, S., Ruzzene, M. and Hanagud, S. (2011), *Computational Techniques for Structural Health*

- Monitoring*, Springer-Verlag London Limited, London, England.
- Grahn, T. (2003), "Lamb wave scattering from a circular partly through-thickness hole in a plate", *Wave Motion*, **37**(1), 63-80. [https://doi.org/10.1016/S0165-2125\(02\)00051-3](https://doi.org/10.1016/S0165-2125(02)00051-3)
- Guo, H.Y., Zhang, L., Zhang, L.L. and Zhou, J.X. (2004), "Optimal placement of sensors for structural health monitoring using improved genetic algorithms", *Smart Mater. Struct.*, **13**(3), 528-534. <https://doi.org/10.1088/0964-1726/13/3/011>
- Hall, J.S., Fromme, P. and Michaels, J.E. (2014), "Guided wave damage characterization via minimum variance imaging with a distributed array of ultrasonic sensors", *J. Nondestruct. Eval.*, **33**(3), 299-308. <https://doi.org/10.1007/s10921-013-0212-x>
- Kammer, D.C. (1991), "Sensor placement for on-orbit modal identification and correlation of large space structures", *J. Guid. Control Dyn.*, **14**(2), 251-259. <https://doi.org/10.2514/3.20635>
- Kay, S.M. (1998), *Fundamentals of Statistical Signal Processing*, Volume 2: Detection Theory, Prentice-Hall and PTR, NJ, USA.
- Kim, S., Lee, J., Wang, H. and Hong, D. (2009), "Sensing performance of energy detector with correlated multiple antennas", *IEEE Signal Process. Lett.*, **16**(8), 671-674. <https://doi.org/10.1109/LSP.2009.2021381>
- Lee, B.C. and Staszewski, W.J. (2007), "Sensor location studies for damage detection with Lamb waves", *Smart Mater. Struct.*, **16**(2), 399-408. <https://doi.org/10.1088/0964-1726/16/2/019>
- Liu, F. (2007), "A general framework for spatial correlation modeling in VLSI design", *Proceedings of the 44th Annual Design Automation Conference*, San Diego, CA, USA, June.
- Liu, W., Gao, W.C., Sun, Y. and Xu, M.J. (2008), "Optimal sensor placement for spatial lattice structure based on genetic algorithms", *J. Sound Vib.*, **317**(1), 175-189. <https://doi.org/10.1016/j.jsv.2008.03.026>
- Liu, X., Zhou, C. and Jiang, Z. (2012), "Damage localization in plate-like structure using built-in PZT sensor network", *Smart Struct. Syst., Int. J.*, **9**(1) 21-33. <https://doi.org/10.12989/sss.2012.9.1.021>
- Mallardo, V., Aliabadi, M.H. and Sharif Khodaei, Z. (2012), "Optimal sensor positioning for impact localization in smart composite panels", *J. Intell. Mater. Syst. Struct.*, **24**(5), 559-573. <https://doi.org/10.1177/1045389X12464280>
- Michaels, J.E. and Michaels, T.E. (2007), "Guided wave signal processing and image fusion for in situ damage localization in plates", *Wave Motion*, **44**(6), 482-492. <https://doi.org/10.1016/j.wavemoti.2007.02.008>
- Michaels, J.E., Hall, J.S. and Michaels, T.E. (2009), "Adaptive imaging of damage from changes in guided wave signals recorded from spatially distributed arrays", *Proceedings of Health Monitoring of Structural and Biological Systems*, Volume 7295, San Diego, CA, USA, March. <https://doi.org/10.1117/12.815849>
- Salmanpour, M., Sharif Khodaei, Z. and Aliabadi, M.H. (2016), "Transducer placement optimisation scheme for a delay and sum damage detection algorithm", *Struct. Control Health Monitor.*, **24**(4), 1-20. <https://doi.org/10.1002/stc.1898>
- Sharif-Khodaei, Z. and Aliabadi, M.H. (2014), "Assessment of delay-and-sum algorithms for damage detection in aluminium and composite plates", *Smart Mater. Struct.*, **23**, 075007. <https://doi.org/10.1088/0964-1726/23/7/075007>
- Shbat, M.S. and Tuzlukov, V. (2013), "Spectrum sensing under correlated antenna array using generalized detector in cognitive radio systems", *Int. J. Antennas Propag.*, **2013**, 1-8. <https://doi.org/10.1155/2013/853746>
- Sun, H. and Büyüköztürk, O. (2015), "Optimal sensor placement in structural health monitoring using discrete optimization", *Smart Mater. Struct.*, **24**(12), 1-16. <https://doi.org/10.1088/0964-1726/24/12/125034>
- Tarhini, H., Itani, R. Fakhri, M.A. and Mustapha, S. (2018), "Optimization of piezoelectric wafer placement for structural health-monitoring applications", *J. Intell. Mater. Syst. Struct.*, **29**(19), 1-16. <https://doi.org/10.1177/1045389X18799204>
- Thiene, M., Sharif Khodaei, Z. and Aliabadi, M.H. (2016), "Optimal sensor placement for maximum area coverage (MAC) for damage localization in composite structures", *Smart Mater. Struct.*, **25**(9), 1-21. <https://doi.org/10.1088/0964-1726/25/9/095037>

- Vanli, O.A., Zhang, C., Nguyen, A. and Wang, B. (2012), "A minimax sensor placement approach for damage detection in composite structures", *J. Intel. Mater. Syst. Struct.*, **23**(8), 919-932.
<https://doi.org/10.1177/1045389X12440751>
- Venkat, R.S., Boller, C., Ravi, N., Chakraborty, N., Kamalakar, G.S., Ukirde, K. and Mahapatra, D.R. (2015), "Optimized actuator/ sensor combinations for structural health monitoring: simulation and experimental validation", In: *International Workshop on Structural Health Monitoring*, Stanford, CA, USA, September.
- Yang, C. (2018), "Sensor placement for structural health monitoring using hybrid optimization algorithm based on sensor distribution index and FE grids", *Struct. Control Health Monitor.*, **25**(6), 1-19.
<https://doi.org/10.1002/stc.2160>
- Yi, T.H., Li, H.N. and Zhang, X.D. (2012a), "A modified monkey algorithm for optimal sensor placement in structural health monitoring", *Smart Mater. Struct.*, **21**(10), 1-9.
<https://doi.org/10.1088/0964-1726/21/10/105033>
- Yi, T.H., Li, H.N. and Zhang, X.D. (2012b), "Sensor placement on Canton Tower for health monitoring using asynchronous-climb monkey algorithm", *Smart Mater. Struct.*, **21**(12), 1-9.
<https://doi.org/10.1088/0964-1726/21/12/125023>
- Yi, T.H., Li, H.N. and Wang, C.W. (2016), "Multiaxial sensor placement optimization in structural health monitoring using distributed wolf algorithm", *Struct. Control Health Monitor.*, **23**(4), 719-734.
<https://doi.org/10.1002/stc.1806>
- Zhou, G.D., Yi, T.H. and Li, H.N. (2014), "Sensor placement optimization in structural health monitoring using cluster-in-cluster firefly algorithm", *Adv. Struct. Eng.*, **17**(8), 1103-1115.
<https://doi.org/10.1260/1369-4332.17.8.1103>